ELSEVIER

Contents lists available at SciVerse ScienceDirect

### Materials Science and Engineering B

journal homepage: www.elsevier.com/locate/mseb



# Effect of addition of aluminum on the evolution of microstructure in HITPERM class Fe<sub>44</sub>Co<sub>44</sub>Zr<sub>7</sub>B<sub>4</sub>Cu<sub>1</sub> alloy

D. Prabhu<sup>a,1</sup>, R. Veerababu<sup>b</sup>, R. Balamuralikrishnan<sup>b</sup>, A. Narayanasamy<sup>c</sup>, K. Chattopadhyay<sup>a,\*</sup>

- <sup>a</sup> Department of Materials Engineering, Indian Institute of Science, Bangalore 560 012, India
- <sup>b</sup> Defence Metallurgical Research Laboratory, Kanchanbagh, Hyderabad 500 058, India
- <sup>c</sup> Materials Science Centre, Department of Nuclear Physics, University of Madras, Guindy Campus, Chennai 600 025, India

#### ARTICLE INFO

Article history: Received 11 July 2011 Received in revised form 25 February 2012 Accepted 18 March 2012 Available online 1 April 2012

Keywords:
Nanocrystallites
Exchange length
Average anisotropy
Permeability
Heterogeneous nucleation

#### ABSTRACT

The paper reports the effect of the addition of small amount of Al on the microstructure and properties of HITPERM class rapidly solidified  $Fe_{44}Co_{44}Zr_7B_4Cu_1$  glassy alloy. Using three dimensional atom probe measurements we present evidence for the formation of Cu clusters on annealing in the metallic glass matrix of the Al containing alloy  $Fe_{43}Co_{43}Al_2Zr_7B_4Cu_1$ . Such clusters are otherwise absent in the parent alloy under similar conditions. The Cu clusters provides heterogeneous nucleation sites for the formation of bcc  $\alpha'$ -FeCo phase leading to an increase in number density of this nanocrystalline phase and thereby enhancing the magnetic properties.

© 2012 Elsevier B.V. All rights reserved.

#### 1. Introduction

Nanocrystalline soft magnetic materials are typically two phase systems comprising of ferromagnetic nanocrystals embedded in ferromagnetic amorphous matrix. Such a microstructure is obtained by the partial devitrification of a precursor glassy alloy obtained by rapid quenching from the melt. The size of the nanocrystals in these alloys are between 7 and 14 nm (ideal for optimal magnetic properties) and is less than the exchange coherence length which is typically in the range of 35-45 nm [1,2]. Due to the ferromagnetic nature of the intermediate glassy matrix, the nanocrystals are exchange coupled and the exchange interaction averages out locally fluctuating anisotropies so that there is only a small net anisotropy effect on the magnetization process. This results in extremely low coercivity and concomitant high permeability and has hence elicited the interests of various researchers in different areas like defense, automotive industry, data storage, etc. [3,4]. Patented alloys FINEMET (Fe-Si-M-B-Cu) [5], NANOP-ERM (Fe-M-B-Cu) [6] and HITPERM (Fe-Co-M-B-Cu) [7] where M = Zr, Mo or Nb, exhibit excellent properties in their own respect.

The formation of these nanocrystallites from the amorphous matrix has attracted considerable attention and extensive

literature is available discussing the mechanism [8], kinetics [9,10] and the role of various elements in the crystallization process [11]. In particular, the role of Cu acting as heterogeneous nucleation sites has been addressed rigorously. Hono et al. observed that copper particles were spatially separated from the  $\alpha$ -Fe particle as revealed in the one-dimensional atom probe concentration depth profile [12]. From extended X-ray absorption fine structure (EXAFS) measurements, Ayers et al. proposed that FCC Cu clusters, which form in the amorphous matrix, provide nucleation sites for the  $\alpha$ -Fe primary particles, and subsequently these clusters are enveloped by the  $\alpha$ -Fe nanocrystals in the microstructure [13]. Hono et al. [14] provided the direct evidence for the presence of copper clusters using three dimensional atom probe (3DAP) technique. They also found that these clusters are present at the interface of the remnant amorphous phase and the  $\alpha$ -Fe nanocrystallite phase. This observation established the role of copper clusters acting as heterogeneous nucleation sites. Zhang et al. [15] reported a similar behavior in the case of NANOPERM type alloys for the formation  $\alpha$ -Fe nanocrystals. However, surprisingly no such Cu clusters could be observed in the case of Zr containing HITPERM type alloys where the crystallizing phase was  $\alpha'$ -(Fe,Co) [16]. Also the fact that there was no obvious difference in grain size between samples with and without Cu ruled out the possibility of Cu acting as heterogeneous nucleation centers in Zr containing HITPERM type alloys.

Our work on Al substitution in FINEMET class of alloys revealed enhanced nucleation with reduced grain size of the FeSi nanocrystallites. This result motivated us to attempt Al substitution in HITPERM class of alloys. The aim of this paper is to study the effect

<sup>\*</sup> Corresponding author. Tel.: +91 80 22932262. E-mail address: kamanio@materials.iisc.ernet.in (K. Chattopadhyay).

<sup>&</sup>lt;sup>1</sup> Present address: National Institute for Materials Science (NIMS), 1-2-1 Sengen, Tsukuba 305-0047, Japan.

of addition of Al on the microstructure and soft magnetic properties of HITPERM alloy.

#### 2. Experimental

Alloys with composition  $Fe_{44}Co_{44}Zr_7B_4Cu_1$ and Fe<sub>43</sub>Co<sub>43</sub>Al<sub>2</sub>Zr<sub>7</sub>B<sub>4</sub>Cu<sub>1</sub> in the form of ingot was obtained by melting high purity metals (at least 99.9% pure) on a water cooled copper hearth using an arc furnace under inert Ar atmosphere. The ingots were melted for at least 4 times to ensure homogenization. The total weight loss of the ingots after melting was found to be less than 0.4%. The alloys were further processed to obtain amorphous ribbons using single wheel melt spinning technique under identical processing conditions. Quartz crucibles and nozzles were used for melt spinning which were carried out under Ar atmosphere using a copper wheel rotating with a linear velocity of 55 m/s. The ribbons were 3-4 mm wide and 20-30 µm thick. Thermal analysis was carried out to follow the transformation behavior using differential scanning calorimeter (DSC) and differential thermal analysis (DTA) (TA make, model Q600). The crystallization temperatures of the amorphous ribbon samples were also determined by studying the variation of electrical resistivity as a function of temperature using a four probe technique by passing 5 mA of current (Sinku-Riko TER-2000). AC initial magnetic permeability of heat-treated samples were determined on magnetically open circuits (ribbon strips) through a conventional fluxmetric technique with air-flux compensation (driving field frequency: 2 kHz, magnetic field: 0.42 A/m) using a lock-in amplifier (PARC-Model: 5209).

Nanocrystalline samples were obtained by heat treating the amorphous ribbons using an infra-red gold image furnace [Sinku Riko make] under a vacuum of  $\sim 10^{-3}$  Pa. The lattice parameter and crystalline volume fraction of the nanocrystallites were determined from X-ray powder patterns obtained using a powder X-ray diffractometer [Heuber, Germany] with Fe-Kα (1.9606 Å) radiation. Atom probe experiments were carried out employing a 3DAP instrument supplied by erstwhile Oxford Nanoscience Ltd., Milton Keynes, UK. To obtain suitable specimens, the as-spun and annealed samples were mechanically polished to  $20 \, \mu m \times 30 \, \mu m \times 6 \, mm$  strips. Sharp tips suitable for atom probe studies were obtained by micro electro polishing technique. Field ion images were recorded at a specimen temperature of 55 K using neon as the imaging gas at  $\sim 2.5 \times 10^{-5}$  mbar pressure. Once a clean field ion image was obtained, the atom probe data acquisition was performed at pressures below  $8 \times 10^{-10}$  mbar at pulse repetition rate of 1 kHz using a 15% pulse fraction. Data reconstruction, analysis, and visualization were performed using the PoSAP software supplied with the instrument.

#### 3. Results

#### 3.1. Thermal analysis

samples of melt spun Fe<sub>44</sub>Co<sub>44</sub>Zr<sub>7</sub>B<sub>4</sub>Cu<sub>1</sub>and Fe<sub>43</sub>Co<sub>43</sub>Al<sub>2</sub>Zr<sub>7</sub>B<sub>4</sub>Cu<sub>1</sub> alloys exhibit a single broad peak in the X-ray diffraction patterns characteristic of a glassy phase. Differential scanning calorimeter (DSC) was used to determine the onset of crystallization in the alloys. Due to the temperature limitation in the DSC, the onset of secondary crystallization was determined using differential thermal analyzer (DTA). The DSC and DTA curves for both the alloys are shown in Fig. 1(a) and (b). It is clear from the two measurements that the onset of primary crystallization  $(T_{x1})$  is lower for Al substituted samples. The activation energy for primary crystallization was determined using the Kissinger method [17] by determining the slope of the plot of  $1000/T_p$  vs  $\ln(\beta/T_p^2)$  where  $T_p$  is the peak temperature of crystallization event

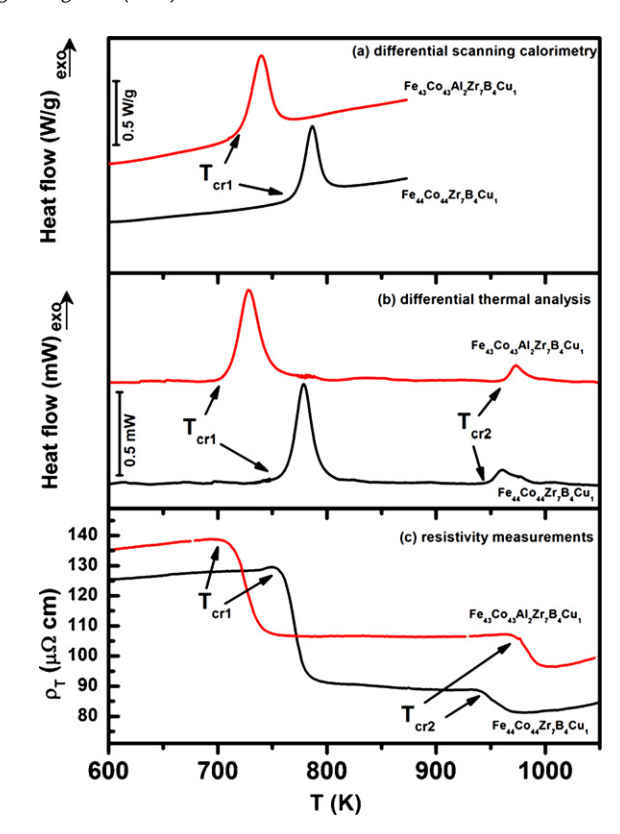


**Fig. 1.** The thermal analysis curves of the two HITPERM samples: (a) DSC showing the suppression of primary crystallization with the addition of 2 at.% Al. (b) DTA curve showing the suppression of the onset of primary crystallization with and without aluminum addition ( $T_{\rm cr1}$ ) and increase in the onset of secondary crystallization ( $T_{\rm cr2}$ ) with addition of 2 at.% Al. (c) Plots showing the change in resistivity as a function of temperature for the two alloys indication the transformation temperatures.

and the  $\beta$  is the heating rate as shown in Fig. 2. The activation energy of 3.54 eV determined for Fe<sub>44</sub>Co<sub>44</sub>Zr<sub>7</sub>B<sub>4</sub>Cu<sub>1</sub> lies within the activation energy range of 2.7–3.8 eV reported for HITPERM alloys by McHenry et al. [9] while the activation energy has decreased to 2.8 eV with Al addition (shown as inset in Fig. 2). In order to further confirm the two crystallization temperatures we have also carried out resistivity measurements as a function of temperature. This is shown in Fig. 1(c). Table 1 summarizes the crystallization

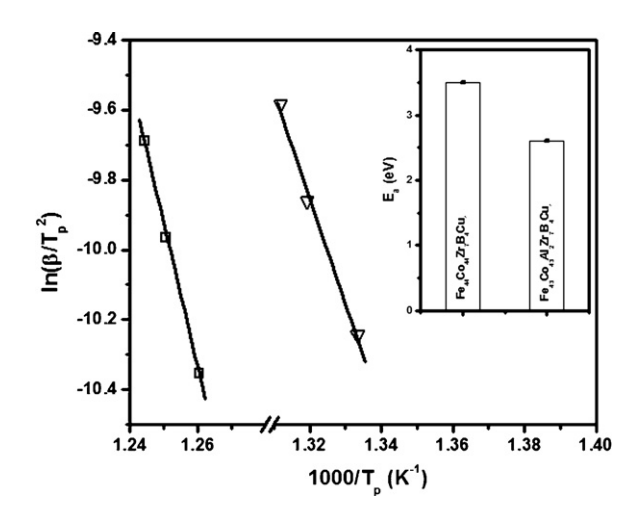


**Fig. 2.** The Kissinger plot for determining the activation energy for the primary crystallization process of  $F_{e44}C_{o44}Z_{r784}C_{u1}$  ( $\square$ ) and  $F_{e43}C_{o43}A_{l2}Z_{r784}C_{u1}$  ( $\triangledown$ ) with inset showing the decrease in activation energy with addition of Al.

#### Download English Version:

## https://daneshyari.com/en/article/1529470

Download Persian Version:

https://daneshyari.com/article/1529470

<u>Daneshyari.com</u>